Forensic Science International 359 (2024) 112026

Contents lists available at ScienceDirect

Forensic Science International

journal homepage: www.elsevier.com/locate/forsciint

Automated reconstruction: Predictive models based on facial morphology matrices

Thandolwethu Mbali Mbonani *, Ericka Noelle L'Abbé, Alison Fany Ridel

University of Pretoria, Department of Anatomy, Faculty of Health Sciences, Tswelopele Building, Private Bag X323, Prinshof 349-Jr, Pretoria 0084, South Africa

ARTICLE INFO

Keywords:
Prediction models
Geometric morphometrics
Hard- and soft-tissue facial morphology matrices
Forensic facial approximation
3D reconstructions

ABSTRACT

Forensic Facial Approximation (FFA) has evolved, with techniques advancing to refine the intercorrelation between the soft-tissue facial profile and the underlying skull. FFA has become essential for identifying unknown persons in South Africa, where the high number of migrant and illegal labourers and many unidentified remains make the identification process challenging. However, existing FFA methods are based on American or European standards, rendering them inapplicable in a South African context. We addressed this issue by conducting a study to create prediction models based on the relationships between facial morphology and known factors, such as population affinity, sex, and age, in white South African and French samples. We retrospectively collected 184 adult cone beam computed tomography (CBCT) scans representing 76 white South Africans (29 males and 47 females) and 108 French nationals (54 males and 54 females) to develop predictive statistical models using a projection onto latent structures regression algorithm (PLSR). On training and untrained datasets, the accuracy of the estimated soft-tissue shape of the ears, eyes, nose, and mouth was measured using metric deviations. The predictive models were optimized by integrating additional variables such as sex and age. Based on trained data, the prediction errors for the ears, eyes, nose, and mouth ranged between 1.6 mm and 4.1 mm for white South Africans; for the French group, they ranged between 1.9 mm and 4.2 mm. Prediction errors on non-trained data ranged between 1.6 mm and 4.3 mm for white South Africans, whereas prediction errors ranging between 1.8 mm and 4.3 mm were observed for the French. Ultimately, our study provided promising predictive models. Although the statistical models can be improved, the inherent variability among individuals restricts the accuracy of FFA. The predictive validity of the models was improved by including sex and age variables and considering population affinity. By integrating these factors, more customized and accurate predictive models can be developed, ultimately strengthening the effectiveness of forensic analysis in the South African region.

1. Introduction

In South Africa's medical-legal laboratories, numerous unidentified remains are discovered annually presenting challenges due to the lack of medical or dental records, fingerprints, DNA, and personal documents [1]. Forensic Facial Approximation (FFA) provides a promising tool for identification in this context, utilizing skull surface analysis and modeling to recreate facial features and improve recognition and potential identification [2–6]. FFA represents the practical application of anatomy and forensic anthropology.

Facial features (i.e., the eyes, ears, nose, and mouth) are crucial for facial recognition [7,8]. In facial approximation, precise eye positioning is crucial for facial recognition due to orbital structure [9–11]. Research emphasizes a supero-lateral eye placement within the orbit, supported by strong evidence [10–13]. Specific distances for these placements, while defined in certain populations, may not directly apply to the South African population [9–11]. Variations in landmark positioning, such as the endocanthion and exocanthion, are also discussed [10,13], providing insights into essential anatomical landmarks for accurate facial reconstruction and their population-specific variability. The human ear is a unique organ that varies distinctly among individuals and population groups [14–16]. Quantitative studies have examined ear morphology, including dimensions, proportions, and bilateral irregularities, aiming to deduce population attributes for anthropological and forensic applications [17,18]. Predictive models for ear shape and dimensions have been developed for FFA [19,20], showing metric variations across individuals and populations, with larger parameters in males and bilateral asymmetry observed. The mouth is a prominent

* Correspondence to: University of Pretoria, Tswelopele Building, Private Bag X323, Prinshof 349-Jr, Pretoria 0084, South Africa.
E-mail addresses: u18059385@tuks.co.za (T.M. Mbonani), ericka.labbe@up.ac.za (E.N. L'Abbé), alisonridel@up.ac.za (A.F. Ridel).

https://doi.org/10.1016/j.forsciint.2024.112026
Received 13 December 2023; Received in revised form 11 April 2024; Accepted 15 April 2024
Available online 16 April 2024

facial area with significant relevance, particularly in FFA [21]. Its positioning plays a crucial role in determining accurate facial proportions [22]. However, there is a discrepancy in mouth approximation techniques, with scholars noting a lack of objectively validated methods for efficient facial approximation [22–24]. The nose is a crucial facial feature with significant diversity, essential for identifying unknown individuals, particularly in facial approximation [25]. Accurate prediction of the nose shape is vital, especially in profile and three-quarter views [7,25]. Research since the 1950 s, inspired by Gerasimov's work, has explored methods to predict nasal projection and shape based on the skeletal structure of the nose [26–29].

The literature explores the complex relationship between underlying skull anatomy and facial surface appearance [30,31]. Gerasimov emphasized the connection between skull relief and soft facial features, showcasing how skull asymmetry is mirrored in facial asymmetry [5]. Skeletal structures form the basis for facial appearance, influencing skin, muscle, fat, and overall appearance [5,32]. Facial approximation involves assessing underlying bone structure, with eye morphology focusing on canthi position and eyeball location within the orbit [24]. Whitnall's (1921) orbit study underpins current standards, noting eyelid margin asymmetry [33]. Nose reconstruction challenges stem from its relationship with surrounding bones [3,30,34], aiming for a wider soft nose than the bony aperture for support without airway obstruction [24]. Mouth morphology interpretation considers teeth alignment, dental patterns, and facial profile [3,35,36]. The ear shape's relationship with skeletal structure lacks comprehensive study [30], with Gerasimov (1955) proposing earlobe attachment correlates with mastoid process orientation [3,37].

Facial structure results from a complex interplay of genetic, hormonal, and environmental factors, shaped by growth patterns and genetic inheritance, alongside influences like age, sex, and population background [38–40]. Dietary habits, muscle activity, and societal trends also contribute significantly to individual facial characteristics [41–43]. Geographical origins and adaptations to diverse climates have influenced facial traits in African, Asian, and European populations [44]. Historical barriers to interracial mating in regions like South Africa, Germany, and the United States have maintained distinct morphological differences [44,45], limiting gene flow and contributing to pronounced variations within and between groups [46]. Forensic anthropology relies on population affinity to construct biological profiles for identifying individuals [44,46], with measurable morphological diversity aiding in forensic identification [44]. Accurately estimating population affinity from skeletal remains guides the selection of the appropriate reference population for estimating other profile aspects such as sex, age, and stature [47]. Sex refers to biological characteristics encompassing genotype, hormonal levels, and anatomy, leading to morphological distinctions between males and females known as sexual dimorphism [48]. Studies highlight the prominence of size in human sexual dimorphism, with males typically exhibiting larger craniofacial dimensions [49–51]. Research comparing North American and South African populations revealed greater cranial size disparities among white South African males and females, emphasizing notable sexual dimorphism [52]. A French study emphasized sexual dimorphism across various facial structures, with discernible differences between males and females [41]. Facial skeletal elements undergo changes in size and shape throughout human development to accommodate growth and maintain functionality [53,54]. The adult face typically undergoes downward and forward growth dynamics, involving resorption of certain facial regions like the canine fossae and nasal aperture [55]. Aging further influences facial morphology through remodeling of hard-tissue structure and alterations in facial musculature due to gravitational effects and dynamic expressions [56,57]. Guyomarc'h et al. [41] demonstrated age-related shape alterations such as thinning of the lips due to tooth loss and changes in the prominence of the nose and chin. Cartilaginous growth in the nose and ears continues into adulthood [58].

The main objective of this study was to construct prediction models that account for the intricate relationship between the morphology of both hard and soft facial tissues and their interdependence on well-established variables such as population affinity, sex, and age.

2. Materials and methods

2.1. Materials

Seventy-six CBCT scans of white South Africans and 108 of French nationals were obtained from the Oral and Dental Hospital (University of Pretoria) and Groenkloof Life Hospital in South Africa, as well as the Pellegrin Hospital Group in Bordeaux, France. The age range for the white South Africans was 18–80 years, while for the French nationals, the age ranged between 18 and 50 years. Additionally, the sample was divided into four age categories: 18 – 29 years old, 30 – 44 years old, 45 – 59 years old, and a group aged 60 years and above. Utilizing a Planmeca ProMax® CBCT scanner with specifications including 90 kV, 11.2 mA, voxel size of 0.4 mm, and field view of 230 ×260 mm, patients were scanned in a seated position, with eyes closed and a relaxed facial expression. All patient data utilized in this study underwent anonymization, retaining only sex, age, and population affinity for analysis. Subjects presenting with conditions potentially impacting facial morphology and subsequent results, such as orthodontic treatment, pathological conditions, facial asymmetry, or facial reconstructive surgery, were excluded from the sample. Approval for the South African sample was obtained from the Research Ethics Committee of the Faculty of Health Sciences at the University of Pretoria, South Africa (Ethics Reference No. 222/2022). Furthermore, for the French sample, approval for the utilization of CBCT data for research purposes was granted by the Pellegrin Hospital Group, Bordeaux, France (Ethics Reference No. DC 2015/172).

2.2. Methods

The CBCT scan images in DICOM format were processed using MeVisLab © v2.7.1 (01–10–2015), a free software platform developed and manufactured by MeVis Medical Solutions AG in Bremen, Germany, for segmentation and the generation of three-dimensional (3D) surface meshes (Fig. 3A). The software interpolated spaces between slices based on a predetermined threshold to create a 3D representation. The "Half Maximum Height" (HMH) quantitative iterative thresholding method was used for segmenting the hard and soft tissue surfaces [59]. The object (hard- or soft-tissue) was segmented into 3D surface meshes [60], which were then saved in a Polygon File Format (ply). In this study, hard-tissue represented the facial skeleton, and soft-tissue represented the external facial features. Structures of hard- and soft-tissue matrices were formed by placing anatomical and sliding landmarks to evaluate shape variation. The utilization of biological landmarks ensured that each identified point was in the same location on all other surfaces in the sample [61]. To ensure homology and comparability between studies, classic definitions of craniometric and capulometric landmarks (types I, II, and III) were utilized [41,61–64]. Overall, 185 landmarks were used in this study, described in Tables 1, 2, and 3 and illustrated in Figs. 1 and 2.

Forty-three craniometric landmarks (Table 1), including 92 sliding landmarks (Table 2) were recorded on the hard-tissue, and 50 capulometric landmarks (Table 3) were recorded on the soft-tissue. These landmarks delineated regions of interest on the facial skeleton and external facial features. The midfacial matrix which comprises of the left and right orbits, left and right nasal bones, anterior nasal aperture, left and right zygoma and left and right maxillae indicated the hard-tissue region of interest (Fig. 1). The exterior curves of the left and right external auditory meatuses (EAM) indicated the regions of interest for the hard-tissue sliding matrices (Fig. 2). Soft-tissue regions of interest included the ears, eyes, nose, and mouth (Fig. 2), with specific bilateral pairs and median landmarks recorded for each. Statistical models were

Table 1
Definitions of craniometric landmarks used for this study [41,64].

No	Landmark	Abbreviation	Nature	Definition
1	Nasion	n	Median	Midline point on the nasofrontal suture.
2	Mid-nasal	mn	Median	Midline point on the internasal suture midway between nasion and rhinion.
3	Rhinion	rhi	Median	Most rostral (end) point on the internasal suture. Cannot be determined accurately if nasal bones are broken distally.
4	Nasospinale	ns	Median	The point where a line drawn between the inferior most points of the nasal aperture cross the median plane. Note that this point is not necessarily at the tip of the nasal spine.
5	Prosthion	pr	Median	Median point between the central incisors on the anterior most margin of the maxillary alveolar rim.
6/7	Zygotemporale superior	zts	Bilateral	Most superior point of the zygomatico-temporal suture.
8/9	Zygotemporale inferior	zti	Bilateral	Most inferior point of the zygomatico-temporal suture.
10/11	Jugale	ju	Bilateral	Vertex of the posterior zygomatic angle, between the vertical edge and horizontal part of the zygomatic arch.
12/13	Frontomalare temporale	fmt	Bilateral	Most lateral part of the zygomaticofrontal suture.
14/15	Frontomalare orbitale	fmo	Bilateral	Point on the orbital rim marked by the zygomaticofrontal suture.
16/17	Nasomaxillofrontale	nmf	Bilateral	Point at the intersection of the frontal, maxillary, and nasal bones.
18/19	Mid-infraorbital	mio	Bilateral	Point on the anterior aspect of the inferior orbital rim, at a line that vertically bisects the orbit.
20/21	Maxilla fronatale	mf	Bilateral	Intersection of the anterior lacrimal crest with the frontomaxillary suture.
22/23	Nasomaxillare	nm	Bilateral	Most inferior point of the nasomaxillary suture on the nasal aperture.
24/25	Alare	al	Bilateral	Instrumentally determined as the most lateral point on the nasal aperture in a transverse plane.
26/27	Piriform curvature	cp	Bilateral	Most infero-lateral point of the piriform aperture.
28/29	Nariale	na	Bilateral	Most inferior point of the piriform aperture.
30/31	Zygomaxillare	zm	Bilateral	Most inferior point on the zygomaticomaxillary suture.
32/33	Supra-canine	sc	Bilateral	Point on the superior alveolar ridge superior to the crown of the maxillary canine.
34/35	Mid-supraorbitale	mso	Bilateral	Point on the anterior aspect of the superior orbital rim, at a line that vertically bisects the orbit.
36/37	Ectoconchion	ec	Bilateral	Lateral point on the orbit at a line that bisects the orbit transversely.
38/39	Medial orbit	mo	Bilateral	Point on the anterior lacrimal crest at the same level as ectoconchion.
40/41	Orbitale	or	Bilateral	Most inferior point of the orbital margin.
42/43	Zygoorbitale	zo	Bilateral	Intersection of the orbital margin and the zygomaticomaxillary suture.

Table 2
Starting point and number of landmarks for each hard-tissue sliding matrix [64].

Matrix	Number of landmarks	Starting point	Definition
Left EAM	46	porion (left)	Most superior point on the upper margin of the external auditory meatus.
Right EAM	46	porion (right)	Most superior point on the upper margin of the external auditory meatus.

developed using hard-tissue configurations to predict soft-tissue shapes (Fig. 2).

2.3. Alignment

The study employed the Frankfurt Horizontal Plane (FHP) to orient the hard-tissue surfaces and Natural Head Position (NHP) to orient the soft-tissue surfaces. The FHP, defined by three osteometric points (both porions and left orbitale), systematically oriented the skull [65], while the highly reproducible NHP ensured consistent landmark placement throughout the study [66,67].

2.4. Automatic landmarking

Automatic landmarking is a non-rigid generic mesh-to-mesh matching algorithm that uses a generated reference template with dense landmarks to associate every point on the reconstructed surfaces (3D images) with the anatomically corresponding point on the reference template [68–70]. This method was first suggested by [71] and has been recently tested by [68]. Fig. 3 displays the modified workflow for the automatic landmarking procedure.

Before registration, all surfaces were adjusted to the same coordinate system, a step known as surface mesh initialization (Fig. 3B). This involved repositioning the floating surface near the target system's coordinate system using affine transformation, manually done in this study. Landmarks on both surfaces were chosen to iteratively rotate and translate them, aligning them closely. These transformations mapped the floating surface's points to the target surface's coordinate space, impacting the subsequent non-rigid surface registration quality.

To align surfaces closely, surface registration is essential [71]. In this study, all surfaces underwent non-rigid registration for statistical 3D shape analysis (Fig. 3C). Each surface consisted of a dense set of interconnected 3D points, ensuring identical numbers of points and connectivity. A standardized reference surface, initially generic, with known point connectivity, was matched to the database surfaces

Table 3
Definition of capulometric landmarks used for this study [41,62–64].

Matrix	No	Landmark	Abbreviation	Position	Definition
Ears	**1**	Tragion	t'	Bilateral	The notch above the tragus where the upper edge of the cartilage disappears into the skin of the face.
	2	Posterotragion	pt'	Bilateral	Most posterior point on the tragus.
	3	Otobasion inferius	obi'	Bilateral	Point of attachment of the ear lobe to the cheek.
	4	Subaurale	sba'	Bilateral	Most inferior point on the free margin of the auricle.
	5	Lobule posterior	lp'	Bilateral	Most posterior point of the lobule where it meets the helix.
	6	Postaurale	pa'	Bilateral	Most posterior point on the free margin of the auricle.
	7	Posterohelixa interna	phi'	Bilateral	Posterior most aspect of the inner helix margin.
	8	Superhelixa interna	shi'	Bilateral	Superior most aspect of the inner helix margin.
	9	Superaurale	sa'	Bilateral	Most superior point on the free margin of the auricle.
	10	Otobasion superius	obs'	Bilateral	Point of attachment of the helix in the temporal region.
	11	Preaurale	pra'	Bilateral	Most anterior point of the ear located just in front of the otobasion superius.
	12	Supraconchale	sc'	Bilateral	Most posterior point of the conchal rim where it crosses under the helix.
	13	Origohelixa	oh'	Bilateral	Point of origin of the helix from the concha.
	14	Antitragion	at'	Bilateral	Apex of the antitragus.
	15	Intertragion	it'	Bilateral	Apex of the groove between the tragus and the antitragus.
	16	Subanguili conchali	iac'	Bilateral	Inferior angle of the conchal rim.
	17	Posterosuperior aurale	psa'	Bilateral	Strongest helical curvature around the midpoint between superaurale and posteroaurale.
	18	Supra-anguili conchali	sac'	Bilateral	Superior angle of the conchal rim.
	19	Strongest anti-helical curvature	shc'	Bilateral	The most posterior point of the conchal rim.
Eyes	**1/2**	Exocanthion	ex'	Bilateral	Lateral point of the outer corner of the eye fissure.
	3/4	Endocanthion	en'	Bilateral	Most medial point of the palpebral fissure, at the inner commissure of the eye; best seen when the subject is gazing upward.
Nose	**1**	Pronasale	prn'	Median	Most anterior midline point of the nose.
	2	Nasale inferius	ni'	Median	Most inferior point of the apex nasi.
	3	Columella	c'	Median	Midpoint of the nasal columella crest, intersecting a line between the two columella points.
	4	Subnasale	sn'	Median	Most postero-superior midline point of the nasal septum.
	5	Sellion	se'	Median	Deepest midline point of the nasofrontal angle.
	6/7	External alar curvature	eac'	Bilateral	Most anterior point of the nasal wing at the maximum of the curvature.
	8/9	Superior alar curvature	sac'	Bilateral	Most superior point of the nasal wing.
	10/11	Alare	al'	Bilateral	The most lateral point on the nasal ala.
	12/13	Alar curvature point	ac'	Bilateral	The most posterolateral point of the curvature of the baseline of each nasal ala.
	14/15	Mid-nostril	mn'	Bilateral	Midpoint of the maximal nostril width –

(*continued on next page*)

Table 3 (*continued*)

Matrix	No	Landmark	Abbreviation	Position	Definition
					projected on the transition nostril/philtrum.
	16/17	Mid-columella	mc'	Bilateral	Midpoint of the nasal columella crest on either side – where the columella thickness is measured.
	18/19	Nasal depth	nd'	Bilateral	Most medial point of the transition nose/eye.
Mouth	**1/2**	Chelion	ch'	Bilateral	Most lateral point of the mouth fissure, where both lips meet.
	3	Labiale superius	ls'	Median	Midpoint of the vermillion border of the upper lip.
	4	Labiale inferius	li'	Median	Midpoint of the vermillion border of the lower lip.
	5/6	Vermillion superius	vs'	Bilateral	Most superior point of the vermillion border of the upper lip at its apex on either side of the mouth.
	7/8	Vermillion inferius	vi'	Bilateral	Most inferolateral point of the vermillion border of the lower lip at the maximum curve change on either side of the mouth.

through dense point correspondences. Consequently, every facial surface in the database was uniformly represented, facilitating the determination of corresponding points across all surfaces. The fundamental idea of automatic landmarking revolves around a reference template depicting the anatomical surface of interest, comprising a dense array of landmarks, which serve as a dense counterpart to traditional sparse, discrete anatomical landmarks. Reference templates for both hard and soft tissues were generated through a non-rigid surface registration procedure (Fig. 3C). For this study, two reference templates were created. For each sample, whether South African or French, had one template individually created and applied to it.

In order to extract shape information, this study employed a landmark-based geometric morphometric (GMM) method to extract and compare details encoded in 3D surface representations. Landmarks positioned on the reference templates were projected onto each subject's surface, establishing a dense point-based anatomical correspondence across all subjects (Fig. 3D-E). GMM facilitated the utilization of geometric data stored within these landmarks, enabling the recording of all landmark coordinates within a shared coordinate system for subsequent statistical analysis.

2.5. Statistical analysis

Firstly, utilizing landmark dispersion, this study compared the reproducibility of 43 craniometric, 50 capulometric, and 92 sliding landmarks to previous research studies [25,69]. Dispersion is the average distance estimated for each landmark and individual between a landmark's mean placement and subsequent placements. The repeatability of landmarks was measured by calculating dispersion Δij for each landmark i and individual j, which is the Mean Euclidean Distance (MED) between landmarks i over every observation k (inter, intra, resp.) for subject j:

$$\Delta_{ij} = \sum_{k=1}^{K} \frac{\left|\left| p_{ijk} - \underline{p}_{ij} \right|\right|}{K}, \text{ with } \sum_{K=1}^{K} \frac{p_{ijk}}{K}$$

Intra-observer errors (INTRA-OE) and inter-observer errors (INTER-OE) between automatic and manual landmarking were used to assess the repeatability of placing landmarks automatically. MeVisLab © v2.7.1 was used for manual landmarking, and ten scans were chosen at random from the whole sample for INTRA-OE and INTER-OE.

Secondly, two separate shape spaces were utilized—one for hard tissue and the other for soft tissue—to create statistical models for predicting soft tissue shape from the underlying hard tissue structure. Both hard and soft tissues were scaled, translated, rotated, and predicted within the same space using hard-tissue information. Firstly, cartesian (x, y, z) coordinates of hard and soft tissue containing information on configurations of landmark shape and size, as well as "nuisance parameters" (orientation and position) were examined using a generalized Procrustes analysis (GPA) to obtain orientation-invariant shape coordinates [72–74] (Fig. 4A). By translating, scaling, and rotating all landmark datasets to the same centroid size, Procrustes shape coordinates were generated, which provide information about the shape of the configurations [75–77]. A PLSR algorithm was applied for extracting information for predicting soft-tissue shape and to select linear combinations required for explaining the predictor variables while maximizing covariation between predictors (hard-tissue shape and additional factors) and response (soft-tissue shape) [78–80] (Fig. 4B). A PLSR employs a linear multivariate model to combine two data matrices, X and Y. Finally, the accuracy of predicting facial soft tissues was evaluated using metric deviations, which allows for future comparison with other research findings. The validation of the prediction models was carried out by estimating the mean square error (MSE) with leave-one-out cross-validation (LOOCV) (Fig. 4C). The estimated MSEs from training and predicted data (RMSE) were compared [81]. The influence of population affinity, sex, and age on the models was evaluated by including these variables as predictors and comparing the resulting MSE. The soft-tissue shape of all specimens from the two population groups was then assessed using a regression model to establish if the covariation was population-dependent.

3. Results

3.1. Reproducibility testing

The average displacement errors of landmarks in the white South African group were generally less than 2 mm for most matrices, except for the left orbit, which had errors less than 3 mm. Table 4 provides detailed data. Regarding soft-tissue configurations, the eyes exhibited the least dispersion for INTRA-OE. For INTER-OE, the mouth displayed the lowest dispersion of landmark placements. The left ear showed the highest INTRA-OE, while the right ear had the highest INTER-OE dispersion. Across all repeatability tests for hard-tissue matrices, the left orbit consistently had the highest dispersion errors for both INTRA-OE and INTER-OE. Conversely, the left EAM exhibited the lowest dispersion for INTER-OE. Lastly, the anterior nasal aperture showed the

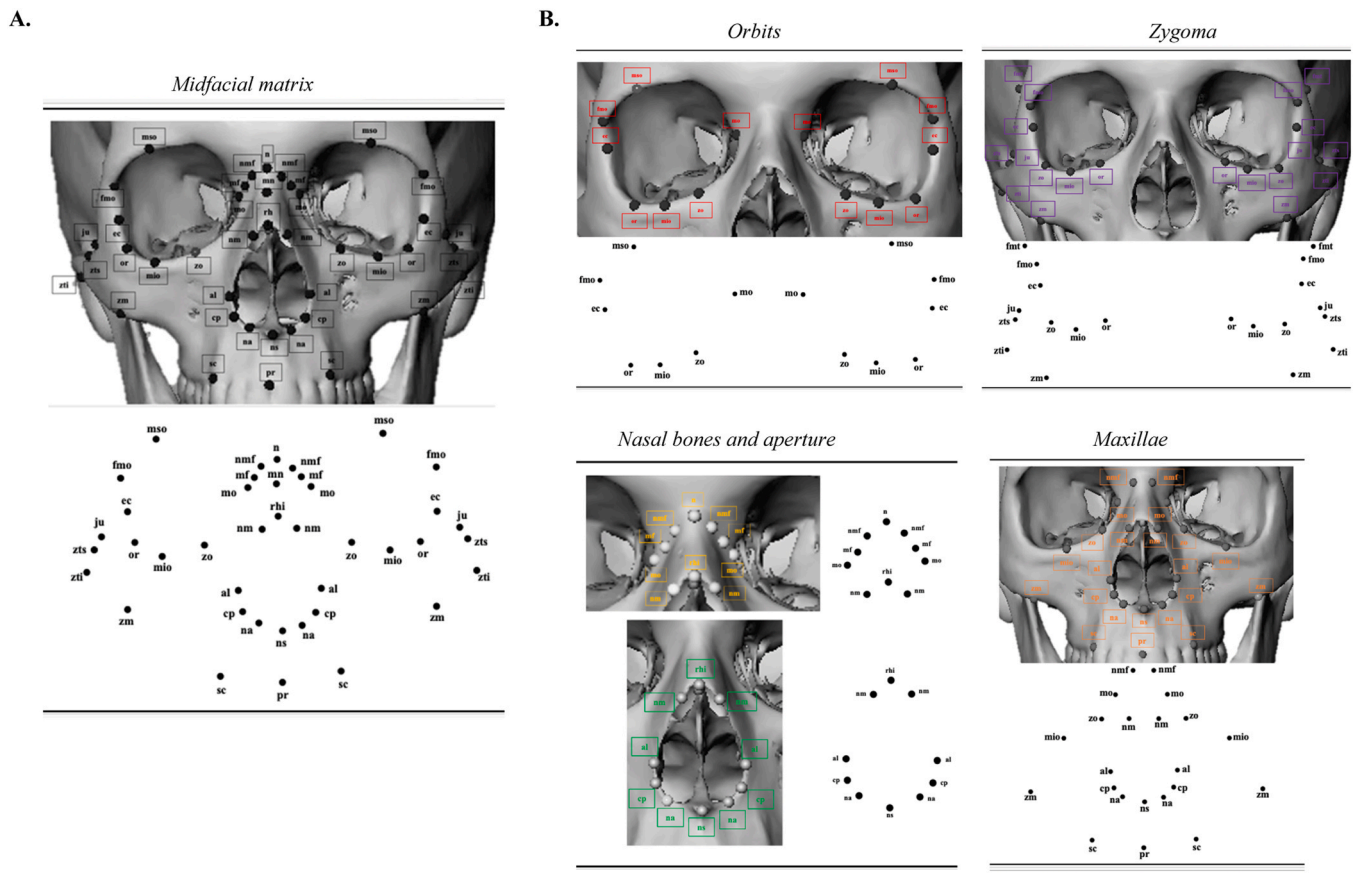

Fig. 1. Hard-tissue region of interest: a) Midfacial matrix, b) Components of the midfacial matrix: orbits (in red), nasal bones (in yellow) and aperture (in green), zygoma (purple), and maxillae (in orange).

lowest INTRA-OE.

The average dispersion error for all capulometric landmarks in the French group was less than 1 mm for both inter- and intra-observations. Regarding craniometric and sliding landmarks on hard-tissue configurations, the mean dispersion error for both INTER-OE and INTRA-OE was less than 2 mm (Table 4). Soft-tissue matrices indicated that the right ear exhibited the highest variation for both INTER-OE and INTRA-OE. Conversely, the eyes had the lowest INTRA-OE, while the mouth had the lowest dispersion of landmark placements for INTER-OE. Craniometric landmarks on the mid-facial matrix displayed similar INTRA-OE and INTER-OE, with the INTRA-OE slightly lower than the INTER-OE. Concerning hard-tissue sliding landmarks, the left EAM had the lowest INTER-OE but the highest INTRA-OE.

3.2. Statistical models

A PLSR model was employed to create a finely tuned prediction system for soft-tissue facial data, using hard-tissue configurations of the EAMs, orbits, and midfacial matrix to estimate the soft-tissue profiles of the ears, eyes, nose, and mouth.

3.3. Ears

In the analysis of the left ear, the white South African group (Table 5) and the French group (Table 6) exhibited errors ranging from 2.1 mm to 2.9 mm (RSMEP = 2.3 mm to 2.7 mm) for trained data (standard deviation [SD] 0.6) and 2.5 mm to 4.1 mm (RSMEP = 3.0 mm to 3.4 mm) for untrained data (SD 1.1). Notably, both sex and age showed comparable prediction errors across both samples. Furthermore, the supraconchale and origohelixa emerged as superior predictors for both populations, demonstrating the lowest prediction errors. For the right ear, average errors ranging from 1.9 mm to 3.0 mm (RSMEP = 2.2 mm to 2.7 mm) were noted for trained data (SD 0.8), and 2.3 mm to 4.2 mm (RSMEP = 2.8 mm to 3.5 mm) for untrained data (SD 0.5) in the white South African (Table 7) and French (Table 8) samples. Moreover, the influence of sex and age proved to improve prediction quality in both populations. Notably, the supraconchale and origohelixa remained the most reliable predictors.

3.4. Eyes

During the analysis of the left eye, the white South African (Table 9) and French (Table 10) groups displayed average errors ranging from 1.6 mm to 4.1 mm (RSMEP = 1.8 mm to 3.7 mm) for trained data (SD 1.8) and 1.6 mm to 4.0 mm (RSMEP = 1.7 mm to 3.6 mm) for untrained data (SD 1.7). The consideration of sex led to enhanced prediction accuracy in both sample sets. Notably, the right endocanthion and exocanthion landmarks emerged as particularly reliable predictors. For the right eye, the white South African (Table 11) and French (Table 12) samples exhibited average errors ranging from 1.9 mm to 4.2 mm (RSMEP = 2.0 mm to 3.8 mm) for trained data (SD 1.6) and 1.8 mm to 4.1 mm (RSMEP = 1.9 mm to 3.6 mm) for untrained data (SD 1.6). The inclusion of sex consistently improved predictions within each sample. Once more, the right endocanthion and exocanthion landmarks emerged as the most reliable predictors.

3.5. Nose

Training data indicated errors ranging from 2.3 mm to 3.0 mm (RSMEP = 2.5 mm to 2.6 mm) (SD 0.5) for the white South African (Table 13) and French (Table 14) groups. Conversely, for untrained data, errors ranged from 2.7 mm to 4.0 mm (RSMEP = 3.1 mm to 3.4 mm)

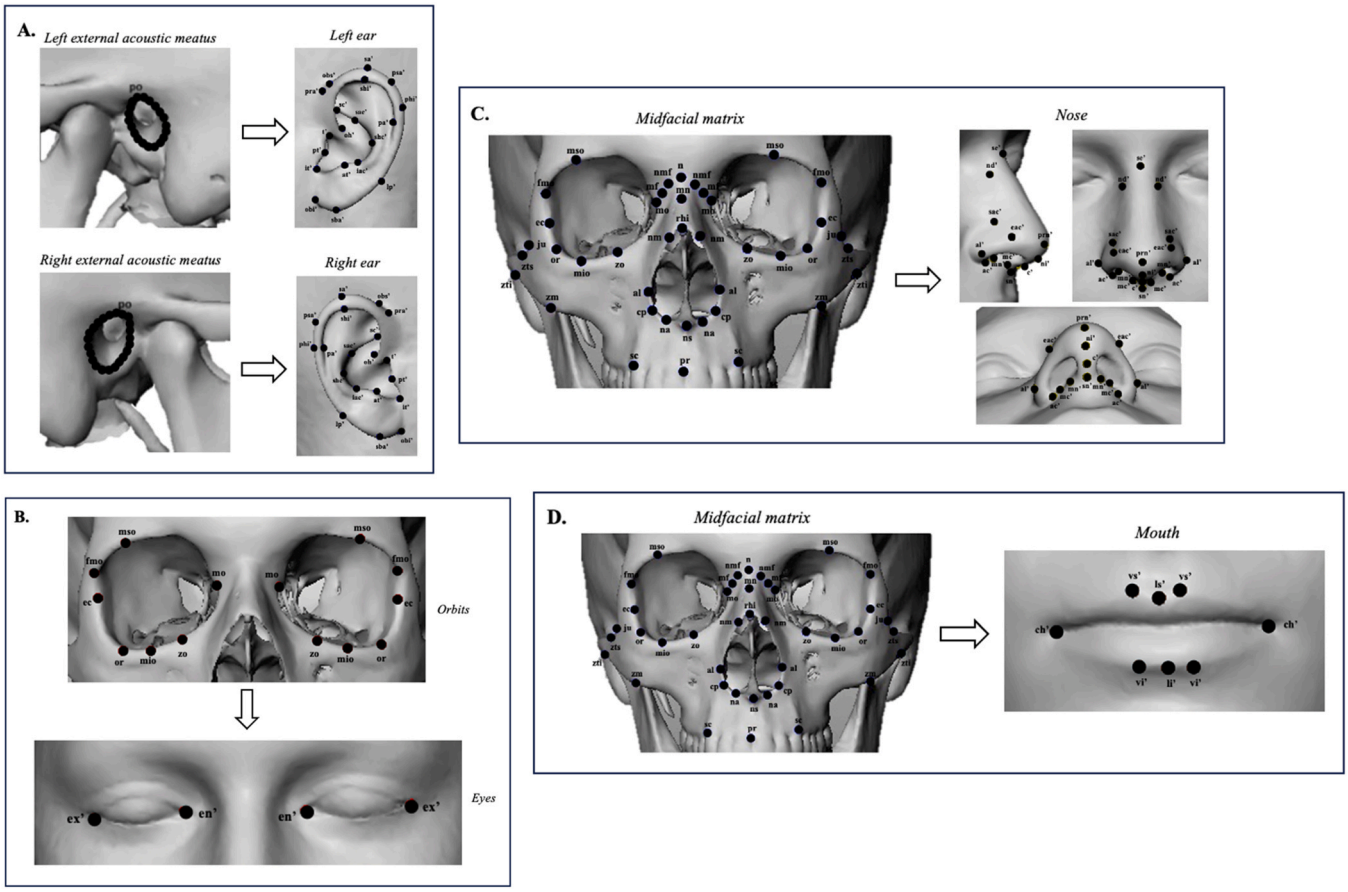

Fig. 2. Hard- and soft-tissue matrices tested in this study for prediction analysis: A. External auditory meatusues and ears B. Orbits and eyes C. Midfacial matrix and nose D. Midfacial matrix and mouth.

(SD 0.9) across both samples. In the white South African and French groups, sex and age exhibited comparable prediction errors. This study also focused on evaluating the average prediction errors of the pronasale and alae, which serve as capulometric landmarks previously examined in nose prediction studies [25,26,29,63]. On training data, the pronasale exhibited errors ranging from 2.5 mm to 3.0 mm (SD 0.2), while on non-trained data, the errors ranged between 3.0 mm and 3.5 mm (SD 0.2) across both samples. For the alae, based on trained data, errors ranging from 3.0 mm to 3.5 mm (SD 0.2) were observed, while untrained data exhibited errors ranging from 2.7 mm to 4.0 mm (SD 0.4).

3.6. Mouth

In the white South African (Table 15) and French (Table 16) samples, training data exhibited errors ranging from 2.6 mm to 3.6 mm (RSMEP = 2.8 mm to 3.6 mm) (SD 0.7). However, for untrained data, the average prediction errors ranged from 3.0 mm to 4.3 mm (RSMEP = 3.5 mm to 3.8 mm) (SD 0.9). As depicted in Tables 15 and 16, both the white South African and French samples showed comparable prediction errors for sex and age. Furthermore, among the facial features evaluated in this study, the mouth displayed the highest overall prediction errors. In the white South African sample (Table 15), the labiale inferius and left vermillion inferius landmarks were superior predictors, while in the French sample (Table 16), the left chelion and left vermillion superius landmarks were better predictors.

Table 17 summarizes the PLSR's predictive performance on predictions obtained from white South African and French models, produced using training and untrained data from the other population. Given that the prediction method was unable to exploit population-specific covariation between both types of tissue, the prediction error was higher for predictions based on the original population database.

4. Discussion

Our research investigated statistical models and the impact of variables (population affinity, sex, and age) on predicting soft-tissue facial morphology based on underlying hard-tissue architecture. Adding age and sex to predictive models for the ears, nose, and mouth in both white South African and French groups notably improved prediction quality, with sex specifically enhancing predictions for the eyes. Our study identified specific anatomical landmarks as better predictors for soft-tissue morphology, such as supraconchale and origohelixa for ear shape in both samples, and endocanthions for eye morphology. Consistent with prior research [3,68], our findings highlighted pronasale and alae positioning as valuable predictors of nose morphology across both samples. Additionally, labiale inferius and left vermillion inferius were effective predictors of mouth shape in the white South African sample, while left chelion and left vermillion superius showed better predictability in the French sample. Several studies have explored the relationship between soft facial contours and the cranial structural framework, influenced by hormonal, genetic, and epigenetic factors, as well as soft tissue development, dental maturation, and biomechanical dynamics [38–40,54]. Facial skeleton components undergo morphological adjustments during human development to maintain functional integrity and proportional growth [38,40,55]. Our study emphasizes that craniofacial development involves bone structure remodeling, suggesting that facial features should not be isolated from the craniofacial skeleton. It highlights the importance of considering population affinity, sex, and age in understanding these morphological changes [57]. The findings highlight notable prediction errors when comparing

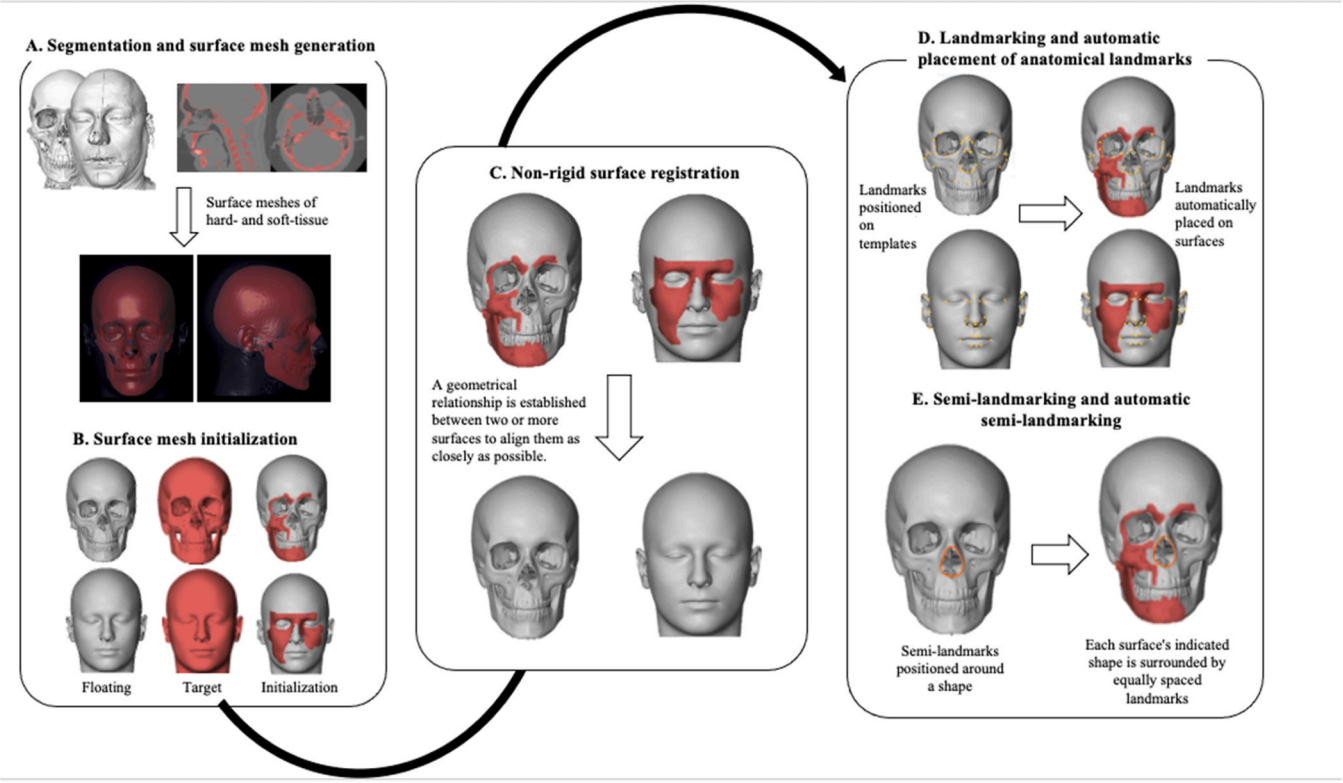

Fig. 3. Workflow of automatic placement of landmarks. A. Segmentation and surface mesh generation B. Surface mesh initialization: repositioning of the floating surface (grey) and the target surface (red) into the same coordinate system (initialization). C. Non-rigid surface registration D. Landmarking and automatic placement of anatomical landmarks E. Semi-landmarking and automatic semi-landmarking.

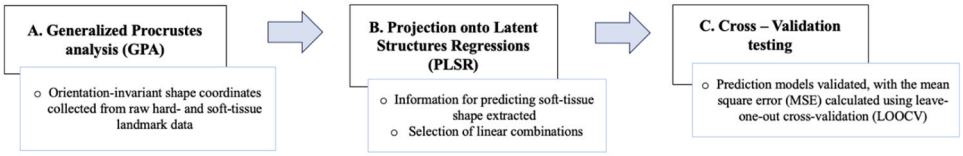

Fig. 4. Creating statistical models to predict facial soft-tissue shape using the underlying hard-tissue configuration.

data from white South Africans with the French group, emphasizing the need for population-specific guidelines in assessing soft-tissue facial morphology and considering population affinity in such analyses. Tailored predictive models were developed to mitigate the impact of population differences. Studies in bioanthropology underscore the substantial influence of environmental factors on facial morphology variation across diverse populations [82–84]. Biological anthropologists have examined morphological diversity among populations using a culturally constructed labeling system to translate biological characteristics [44, 85]. Population affinity presents a complex aspect of a biological profile, integrating societal norms, environmental variables, and biological characteristics, which allows forensic anthropologists to categorize unknown deceased individuals into populations most similar to them [47].

Sexual dimorphism notably impacted prediction accuracy for the ears, nose, and mouth in both the white South African and French samples, with notable improvements observed for the eyes. Guyomarc'h et al. [41] introduced a computerized technique using GMM to estimate facial morphology in a French sample, emphasizing the impact of sex on craniofacial structure in facial approximation models. Moreover, similar sexually dimorphic patterns were observed in the nasal, buccal, and auditory regions across craniometric and capulometric landmark groups. South African studies [47,83,86] using traditional morphometric techniques demonstrated substantial sexual dimorphism in craniofacial morphology, affecting both size and shape. In FFA, distinguishing between male and female faces based on facial shape and size is crucial for accurate facial approximations [52,87]. Our observations also indicate that aging notably affects the prediction accuracy of the ears, nose, and mouth. With advancing age, the facial skeleton tends to adopt a more convex shape, while soft tissues become more prominent, resulting in nasal and auricular growth, as well as elongation of the mouth [57,88]. Biochemical changes in connective tissue reduce skin elasticity, affecting adherence to underlying bone or musculature [89]. Bone resorption and tooth loss modify jawline and mouth contours [90]. Nasal and chin prominence increases with age, reducing the distance between them and making the mouth appear sunken [58]. Cartilaginous nose and ear segments continue to grow throughout adulthood, contributing to predictable changes in facial shape and size influenced by biological and environmental factors [58]. Moreover, our findings highlight the importance of age and sex in improving predictive quality. However, inherent human variation poses challenges to the accuracy of facial approximation. To address this, our study recommends including more diverse demographic groups in reference samples, such as black and coloured South Africans, along with incorporating new measures such as soft tissue thickness values, craniometrics, corpulence etc. to enhance model reliability. While our study highlighted the importance of variables like sex in improving prediction accuracy for specific facial

Table 4
Mean (M) and standard deviation (SD) of the dispersion errors for soft- and hard-tissue landmarks and hard-tissue sliding landmarks in the French sample and white South African sample.

		French sample				White South African sample			
		INTRA-OE		INTER-OE		INTRA-OE		INTER-OE	
		M	SD	M	SD	M	SD	M	SD
Soft-tissue	Left ear	0.9	0.3	0.7	0.2	1.0	0.4	1.3	0.7
	Right ear	1.0	0.2	0.9	0.3	0.8	0.3	1.7	0.8
	Eyes	0.6	0.1	0.4	0.1	0.4	0.0	1.2	0.7
	Nose	0.8	0.1	0.7	0.1	0.8	0.2	1.1	0.5
	Mouth	0.5	0.2	0.5	0.2	0.6	0.1	1.1	0.5
Hard-tissue	Midfacial matrix	1.0	0.1	0.9	0.1	0.8	0.1	1.1	0.2
	Left EAM	2.0	0.0	0.4	0.2	0.8	0.0	0.4	0.2
	Right EAM	1.3	0.1	2.0	0.1	0.5	0.0	0.5	0.1
	Left orbit	3.4	2.1	3.3	2.2	2.1	0.1	1.6	0.1
	Right orbit	2.3	0.1	2.0	0.1	1.0	0.0	1.5	0.1
	Nasal aperture	0.4	0.1	0.7	0.1	0.3	0.1	0.9	0.2

Dispersion mean values < 2 mm indicate a significant degree of dependability and consistency in the automated landmarking process. M, representing the mean; SD, denoting the standard deviation; and EAM, referring to the external acoustic meatus.

features such as the eyes, it is crucial to recognize the broader benefits of incorporating multiple variables like sex and age when constructing prediction models. Firstly, this approach enhances accuracy by comprehensively analyzing various factors influencing facial morphology, leading to more precise predictions compared to single-variable models. Secondly, using multiple variables reduces potential biases, promoting fairer and more reliable analyses. Additionally, prediction models with multiple variables demonstrate greater generalizability across diverse populations or contexts, considering a wider spectrum of influencing factors.

Statistical models tailored to specific populations were developed for the ears, eyes, nose, and mouth, yielding errors when applied to non-trained data using landmark-to-landmark distances. Currently, there is a scarcity of scientific literature focusing on soft-tissue predictions of facial regions based on landmark-to-landmark distances, similar to the methods outlined in this study, as evidenced by [25,41,63,91,92]. In the case of the ears, the prediction errors ranged between 1.9 mm and 3.8 mm for white South Africans and from 2.3 mm to 4.2 mm for the French sample. Guyomarc'h [41] reported prediction errors ranging from 4.7 mm to 8.3 mm based on point-to-point distances for the auditory matrix. For the eyes, prediction errors fell within the range of 1.6 mm to 4.2 mm for the exocanthion and endocanthion in the white South African and French samples. Guyomarc'h noted errors ranging from 2.6 mm to 3.2 mm for the endocanthion and exocanthion in the optical subset [41]. In terms of the nose, errors for the pronasale and alae among white South Africans ranged from 2.3 mm to 3.9 mm, whereas the French sample exhibited errors ranging from 2.4 mm to 4.0 mm. In Ridel's study [25], the error distribution based on landmark-to-landmark distances revealed errors ranging from 2.0 mm to 2.6 mm around the pronasale and from 2.0 to 2.9 mm for the alae. Tilotta et al. [91] documented an average error of merely 1 mm, determined through point-to-mesh distances, across a subset of 49 specimens spanning the entire surface. Vandermeulen et. al [92] revealed an error distribution based on mesh-to-mesh distances, with errors ranging from 2.0 to 2.5 mm around the pronasale and from 1 to 2 mm for the alae. Guyomarc'h [41] found prediction errors between 2.7 and 3.1 mm for the respiratory matrix based on point-to-point distances [41]. Schlager [63] presents prediction errors ranging from 1.2 to 1.4 mm when utilizing mesh-to-mesh distances. Additionally, Schlager [63] conducted separate analyses for two population groups (Chinese and European). In the European sample, prediction errors ranged between 2.2 mm and 2.7 mm at the alae and pronasale, whereas they varied from 2.0 mm to 2.4 mm for the Chinese subsample. For the mouth, both the white South African and French groups demonstrated errors between 2.7 mm to 4.3 mm. Guyomarc'h found prediction errors between 4.1 mm to 4.8 mm for the buccal matrix [41]. Tilotta [91] and Vandermeulen [92] employed different methodologies compared to our study, focusing on distinct facial regions. Our study aligns closely with approaches by Schlager [63], Guyomarc'h [41] and Ridel [25], emphasizing the delineation of biologically relevant substructures using landmarks [25,41] and semi-landmarks [63]. Areas of the face with underlying bone structure tend to yield more accurate predictions, a similarity noted in these studies.

Our study encountered challenges in comparing with existing literature due to the limited research specifically focused on prediction models for individual facial features such as the eyes, nose, mouth, and

Table 5
Prediction errors (in mm) of the predicted capulometric landmarks of the **left ear** in the white South African sample, calculated on 76 individuals, based on training and on non-trained data.

White South Africans			Plain		Sex		Age		Sex*Age	
Predicted capulometric landmarks			PE	**PE**_cv	PE	**PE**_cv	PE	**PE**_cv	PE	**PE**_cv
Left ear	**1**	*Tragion*	2.5	3.0	**2.4**	**2.9**	**2.4**	**3.0**	2.4	2.9
	2	*Posterotragion*	2.4	3.5	**2.4**	**3.5**	**2.4**	**3.3**	2.3	3.5
	3	*Otobasion inferius*	2.6	3.3	**2.6**	**3.2**	**2.5**	**3.0**	2.5	3.1
	4	*Subaurale*	2.3	3.0	**2.3**	**2.9**	**2.3**	**2.9**	2.3	2.9
	5	*Lobule posterior*	2.5	3.6	**2.5**	**3.6**	**2.4**	**3.4**	2.4	3.7
	6	*Postaurale*	2.6	3.3	**2.6**	**3.2**	**2.5**	**3.0**	2.5	3.1
	7	*Posterohelixa interna*	2.3	2.9	**2.3**	**2.8**	**2.3**	**2.8**	2.2	2.7
	8	*Superhelixa interna*	2.6	3.7	**2.6**	**3.6**	**2.5**	**3.5**	2.6	3.7
	9	*Superaurale*	2.3	3.0	**2.3**	**2.9**	**2.3**	**2.8**	2.2	2.8
	10	*Otobasion superius*	2.3	2.9	**2.3**	**2.8**	**2.3**	**2.9**	2.3	2.7
	11	*Preaurale*	2.6	3.6	**2.6**	**3.6**	**2.5**	**3.6**	2.6	3.8
	12	*Supraconchale*	2.2	2.8	**2.2**	**2.7**	**2.1**	**2.6**	2.2	2.6
	13	*Origohelixa*	2.1	2.6	**2.1**	**2.5**	**2.1**	**2.6**	2.1	2.5
	14	*Antitragion*	2.6	3.6	**2.6**	**3.6**	**2.5**	**3.5**	2.6	3.7
	15	*Intertragion*	2.3	3.0	**2.3**	**3.0**	**2.3**	**2.9**	2.3	2.8
	16	*Subanguili conchali*	2.3	2.9	**2.3**	**2.9**	**2.3**	**2.7**	2.3	2.7
	17	*Posterosuperior aurale*	2.3	2.9	**2.3**	**2.8**	**2.3**	**2.8**	2.3	2.8
	18	*Supra-anguili conchali*	2.4	2.9	**2.4**	**2.9**	**2.4**	**2.9**	2.4	2.9
	19	*Strongest anti-helical curvature*	2.2	3.2	**2.2**	**3.2**	**2.2**	**3.0**	2.2	3.2
		RMSEP	2.4	3.1	**2.4**	**3.1**	**2.3**	**3.0**	2.4	3.1

PE: Prediction errors on training data; PE_cv: prediction errors on non-trained data. Better predictions are indicated in bold.

Table 6
Prediction errors (in mm) of the predicted capulometric landmarks of the **left ear** in the French sample, calculated on 108 individuals, based on training and on non-trained data.

French			Plain		Sex		Age		Sex*Age	
Predicted capulometric landmarks			PE	**PE**_cv	PE	**PE**_cv	PE	**PE**_cv	PE	**PE**_cv
Left ear	**1**	*Tragion*	2.7	3.2	**2.7**	**3.2**	**2.7**	**3.2**	2.6	3.1
	2	*Posterotragion*	2.6	3.7	**2.6**	**3.7**	**2.6**	**3.6**	2.6	3.7
	3	*Otobasion inferius*	2.9	3.5	**2.9**	**3.5**	**2.7**	**3.3**	2.8	3.4
	4	*Subaurale*	2.6	3.2	**2.6**	**3.1**	**2.6**	**3.2**	2.6	3.1
	5	*Lobule posterior*	2.7	3.9	**2.7**	**3.9**	**2.7**	**3.7**	2.7	3.9
	6	*Postaurale*	2.9	3.6	**2.9**	**3.5**	**2.7**	**3.3**	2.7	3.3
	7	*Posterohelixa interna*	2.6	3.1	**2.5**	**3.1**	**2.5**	**3.1**	2.5	3.0
	8	*Superhelixa interna*	2.8	3.9	**2.8**	**3.9**	**2.8**	**3.8**	2.8	4.0
	9	*Superaurale*	2.6	3.2	**2.6**	**3.2**	**2.5**	**3.0**	2.5	3.0
	10	*Otobasion superius*	2.6	3.1	**2.6**	**3.1**	**2.6**	**3.1**	2.6	3.0
	11	*Preaurale*	2.8	3.9	**2.8**	**3.9**	**2.8**	**3.8**	2.8	4.1
	12	*Supraconchale*	2.5	3.1	**2.5**	**3.0**	**2.4**	**2.8**	2.4	2.9
	13	*Origohelixa*	2.4	2.9	**2.4**	**2.8**	**2.4**	**2.8**	2.4	2.7
	14	*Antitragion*	2.8	3.9	**2.8**	**3.9**	**2.8**	**3.8**	2.8	4.0
	15	*Intertragion*	2.6	3.2	**2.6**	**3.2**	**2.6**	**3.2**	2.5	3.1
	16	*Subanguili conchali*	2.6	3.2	**2.6**	**3.2**	**2.5**	**3.0**	2.5	3.0
	17	*Posterosuperior aurale*	2.6	3.2	**2.6**	**3.1**	**2.6**	**3.1**	2.5	3.0
	18	*Supra-anguili conchali*	2.7	3.2	**2.7**	**3.2**	**2.7**	**3.2**	2.6	3.1
	19	*Strongest anti-helical curvature*	2.5	3.5	**2.5**	**3.4**	**2.4**	**3.3**	2.5	3.4
		RMSEP	2.7	3.4	**2.6**	**3.4**	**2.6**	**3.3**	2.6	3.3

PE: Prediction errors on training data; PE_cv: prediction errors on non-trained data. Better predictions are indicated in bold.

Table 7
Prediction errors (in mm) of the predicted capulometric landmarks of the **right ear** in the white South African sample, calculated on 76 individuals, based on training and on non-trained data.

White South African			Plain		Sex		Age		Sex*Age	
Predicted capulometric landmarks			PE	**PE**_cv	PE	**PE**_cv	PE	**PE**_cv	PE	**PE**_cv
Right ear	**1**	*Tragion*	2.3	2.8	**2.3**	**2.8**	**2.2**	**2.8**	2.2	2.7
	2	*Posterotragion*	2.2	3.3	**2.2**	**3.3**	**2.2**	**3.1**	2.1	3.3
	3	*Otobasion inferius*	2.4	3.1	**2.4**	**3.0**	**2.3**	**2.8**	2.3	2.9
	4	*Subaurale*	2.1	2.8	**2.1**	**2.7**	**2.1**	**2.7**	2.1	2.7
	5	*Lobule posterior*	2.3	3.4	**2.3**	**3.4**	**2.2**	**3.3**	2.2	3.5
	6	*Postaurale*	2.4	3.1	**2.4**	**3.1**	**2.3**	**2.9**	2.3	2.9
	7	*Posterohelixa interna*	2.1	2.7	**2.1**	**2.6**	**2.1**	**2.6**	2.1	2.5
	8	*Superhelixa interna*	2.4	3.5	**2.4**	**3.4**	**2.4**	**3.3**	2.4	3.5
	9	*Superaurale*	2.1	2.8	**2.1**	**2.7**	**2.1**	**2.6**	2.1	2.6
	10	*Otobasion superius*	2.1	2.7	**2.1**	**2.6**	**2.1**	**2.7**	2.1	2.6
	11	*Preaurale*	2.4	3.5	**2.4**	**3.5**	**2.3**	**3.4**	2.4	3.6
	12	*Supraconchale*	2.0	2.6	**2.0**	**2.5**	**1.9**	**2.4**	2.0	2.4
	13	*Origohelixa*	1.9	2.4	**1.9**	**2.4**	**1.9**	**2.4**	1.9	2.3
	14	*Antitragion*	2.4	3.5	**2.4**	**3.4**	**2.3**	**3.3**	2.4	3.5
	15	*Intertragion*	2.1	2.8	**2.1**	**2.8**	**2.1**	**2.7**	2.1	2.6
	16	*Subanguili conchali*	2.1	2.7	**2.1**	**2.7**	**2.1**	**2.5**	2.1	2.6
	17	*Posterosuperior aurale*	2.1	2.7	**2.1**	**2.7**	**2.1**	**2.6**	2.1	2.6
	18	*Supra-anguili conchali*	2.3	2.7	**2.3**	**2.7**	**2.2**	**2.7**	2.2	2.7
	19	*Strongest anti-helical curvature*	2.1	3.0	**2.0**	**3.0**	**2.0**	**2.8**	2.0	3.0
		RMSEP	2.2	2.9	**2.2**	**2.9**	**2.2**	**2.8**	2.2	2.9

PE: Prediction errors on training data; PE_cv: prediction errors on non-trained data. Better predictions are indicated in bold.

ears. While extensive research exists on facial recognition and analysis, including prediction models for overall facial structure or specific landmarks, there is a notable gap in studies addressing distinct facial features. This gap highlights the need for further exploration into developing and refining prediction models for individual facial attributes. Addressing this gap could enhance our understanding of facial morphology and improve the accuracy and applicability of facial recognition technologies.

The population-specific predictive models developed in this study show promise, with an average prediction error of about 3–4 mm, which is deemed acceptable [41]. Guyomarc'h et al. [41] evaluated prediction accuracy by compiling a full set of landmarks for estimating sensory landmarks in 500 French individuals, enabling calculation of average distances between true and estimated landmarks through leave-one-out resampling. Reconstruction uncertainty varied across facial regions, notably high for the ear (7 mm), moderate for the mouth (4.5 mm), and relatively lower for the nasal (3.1 mm) and eye (2.9 mm) regions [41]. Our models suggest potential for improved facial approximations, with relatively low average errors; however, caution is advised in cross-study comparisons due to variations in measurement methods like mesh-to-mesh distance [92], point-to-mesh distance [63,91], or point-to-point distance [25,41,63]. Independent validation of our approach using separate samples is imperative.

5. Conclusion

Our research introduces a novel facial approximation method using geometric morphometrics to estimate soft-tissue facial morphology in white South Africans and French individuals. These prediction models have critical applications in forensic facial approximations and anthropology, enabling precise facial estimates from skeletal remains to enhance identification accuracy. By incorporating population-specific

Table 8
Prediction errors (in mm) of the predicted capulometric landmarks of the **right ear** in the French sample, calculated on 108 individuals, based on training and on non-trained data.

French			Plain		Sex		Age		Sex*Age	
Predicted capulometric landmarks			PE	**PE**_cv	PE	**PE**_cv	PE	**PE**_cv	PE	**PE**_cv
Right ear	**1**	*Tragion*	2.8	3.3	**2.8**	**3.3**	**2.8**	**3.3**	2.7	3.2
	2	*Posterotragion*	2.7	3.8	**2.7**	**3.8**	**2.7**	**3.6**	2.7	3.8
	3	*Otobasion inferius*	3.0	3.6	**3.0**	**3.6**	**2.8**	**3.4**	2.8	3.4
	4	*Subaurale*	2.7	3.3	**2.7**	**3.2**	**2.6**	**3.3**	2.7	3.2
	5	*Lobule posterior*	2.8	3.9	**2.8**	**4.0**	**2.8**	**3.8**	2.8	4.0
	6	*Postaurale*	3.0	3.7	**3.0**	**3.6**	**2.8**	**3.4**	2.8	3.4
	7	*Posterohelixa interna*	2.6	3.2	**2.6**	**3.2**	**2.6**	**3.2**	2.6	3.1
	8	*Superhelixa interna*	2.9	4.0	**2.9**	**4.0**	**2.9**	**3.9**	2.9	4.1
	9	*Superaurale*	2.7	3.3	**2.7**	**3.2**	**2.6**	**3.1**	2.6	3.1
	10	*Otobasion superius*	2.7	3.2	**2.7**	**3.1**	**2.7**	**3.2**	2.7	3.1
	11	*Preaurale*	2.9	4.0	**2.9**	**4.0**	**2.9**	**3.9**	2.9	4.2
	12	*Supraconchale*	2.5	3.2	**2.5**	**3.1**	**2.5**	**2.9**	2.5	3.0
	13	*Origohelixa*	2.5	2.9	**2.5**	**2.9**	**2.5**	**2.9**	2.4	2.8
	14	*Antitragion*	2.9	4.0	**2.9**	**3.9**	**2.9**	**3.8**	2.9	4.1
	15	*Intertragion*	2.7	3.3	**2.7**	**3.3**	**2.6**	**3.2**	2.6	3.1
	16	*Subanguili conchali*	2.7	3.2	**2.7**	**3.3**	**2.6**	**3.1**	2.6	3.1
	17	*Posterosuperior aurale*	2.7	3.2	**2.7**	**3.2**	**2.6**	**3.2**	2.6	3.1
	18	*Supra-anguili conchali*	2.8	3.3	**2.8**	**3.3**	**2.8**	**3.3**	2.7	3.2
	19	*Strongest anti-helical curvature*	2.6	3.6	**2.6**	**3.5**	**2.5**	**3.4**	2.5	3.5
		RMSEP	2.7	3.5	**2.7**	**3.4**	**2.7**	**3.4**	2.7	3.4

PE: Prediction errors on training data; PE_cv: prediction errors on non-trained data. Better predictions are indicated in bold.

Table 9
Prediction errors (in mm) of the predicted capulometric landmarks of the **left eye** in the white South African sample, calculated on 76 individuals, based on training and on non-trained data.

White South African			Plain		Sex		Age		Sex*Age	
Predicted capulometric landmarks			PE	**PE**_cv	PE	**PE**_cv	PE	**PE**_cv	PE	**PE**_cv
Left eye	**1**	*Exocanthion L*	2.0	1.9	**1.9**	**1.8**	3.2	3.2	3.9	3.7
	2	*Exocanthion R*	2.0	1.9	**1.9**	**1.8**	2.7	2.7	3.3	3.1
	3	*Endocanthion L*	2.0	1.9	**1.8**	**1.7**	3.0	3.0	3.7	3.6
	4	*Endocanthion R*	1.9	1.8	**1.6**	**1.6**	2.6	2.6	3.0	2.9
		RMSEP	2.0	1.9	**1.8**	**1.7**	2.9	2.9	3.5	3.3

PE: Prediction errors on training data; PE_cv: prediction errors on non-trained data. Better predictions are indicated in bold.

Table 10
Prediction errors (in mm) of the predicted capulometric landmarks of the **left eye** in the French sample, calculated on 108 individuals, based on training and on non-trained data.

French			Plain		Sex		Age		Sex*Age	
Predicted capulometric landmarks			PE	**PE**_cv	PE	**PE**_cv	PE	**PE**_cv	PE	**PE**_cv
Left eye	**1**	*Exocanthion L*	2.3	2.2	**2.2**	**2.0**	3.5	3.5	4.1	4.0
	2	*Exocanthion R*	2.2	2.2	**2.1**	**2.1**	3.0	3.0	3.5	3.4
	3	*Endocanthion L*	2.2	2.1	**2.0**	**2.0**	3.3	3.3	3.9	3.8
	4	*Endocanthion R*	2.2	2.0	**1.9**	**1.8**	2.8	2.8	3.2	3.1
		RMSEP	2.2	2.1	**2.1**	**2.0**	3.1	3.1	3.7	3.6

PE: Prediction errors on training data; PE_cv: prediction errors on non-trained data. Better predictions are indicated in bold.

Table 11
Prediction errors (in mm) of the predicted capulometric landmarks of the **right eye** in the white South African sample, calculated on 76 individuals, based on training and on non-trained data.

White South African			Plain		Sex		Age		Sex*Age	
Predicted capulometric landmarks			PE	**PE**_cv	PE	**PE**_cv	PE	**PE**_cv	PE	**PE**_cv
Right eye	**1**	*Exocanthion L*	2.2	2.1	**2.1**	**2.0**	3.4	3.4	4.1	4.0
	2	*Exocanthion R*	2.2	2.1	**2.1**	**2.1**	2.9	2.9	3.5	3.4
	3	*Endocanthion L*	2.2	2.1	**2.0**	**1.9**	3.2	3.2	3.9	3.8
	4	*Endocanthion R*	2.1	2.0	**1.9**	**1.8**	2.8	2.8	3.2	3.1
		RMSEP	2.2	2.1	**2.0**	**1.9**	3.1	3.1	3.7	3.5

PE: Prediction errors on training data; PE_cv: prediction errors on non-trained data. Better predictions are indicated in bold.

Table 12
Prediction errors (in mm) of the predicted capulometric landmarks of the **right eye** in the French sample, calculated on 108 individuals, based on training and on non-trained data.

French			Plain		Sex		Age		Sex*Age	
Predicted capulometric landmarks			PE	**PE**_cv	PE	**PE**_cv	PE	**PE**_cv	PE	**PE**_cv
Right eye	**1**	*Exocanthion L*	2.3	2.2	**2.2**	**2.1**	3.5	3.5	4.2	4.1
	2	*Exocanthion R*	2.3	2.2	**2.2**	**2.2**	3.0	3.0	3.6	3.5
	3	*Endocanthion L*	2.3	2.2	**2.1**	**2.0**	3.3	3.3	4.0	3.9
	4	*Endocanthion R*	2.2	2.1	**2.0**	**1.9**	2.9	2.9	3.3	3.2
		RMSEP	2.3	2.2	**2.1**	**2.0**	3.2	3.2	3.8	3.6

PE: Prediction errors on training data; PE_cv: prediction errors on non-trained data. Better predictions are indicated in bold.

Table 13
Prediction errors (in mm) of the predicted capulometric landmarks of the **nose** in the white South African sample, calculated on 76 individuals, based on training and on non-trained data.

White South Africans			Plain		Sex		Age		Sex*Age	
Predicted capulometric landmarks			PE	**PE**_cv	PE	**PE**_cv	PE	**PE**_cv	PE	**PE**_cv
Nose	**1**	*Pronasale*	2.6	3.1	**2.6**	**3.1**	**2.6**	**3.1**	2.5	3.0
	2	*Nasale inferius*	2.5	3.6	**2.5**	**3.6**	**2.5**	**3.4**	2.5	3.6
	3	*Columella*	2.7	3.4	**2.7**	**3.4**	**2.6**	**3.2**	2.6	3.2
	4	*Subnasale*	2.5	3.1	**2.4**	**3.0**	**2.4**	**3.1**	2.4	3.0
	5	*Sellion*	2.6	3.7	**2.6**	**3.8**	**2.6**	**3.6**	2.6	3.8
	6	*External alar curvature L*	2.7	3.4	**2.7**	**3.4**	**2.6**	**3.2**	2.6	3.2
	7	*External alar curvature R*	2.4	3.0	**2.4**	**3.0**	**2.4**	**3.0**	2.4	2.9
	8	*Superior alar curvature L*	2.7	3.8	**2.7**	**3.8**	**2.7**	**3.6**	2.7	3.9
	9	*Superior alar curvature R*	2.5	3.1	**2.5**	**3.0**	**2.4**	**2.9**	2.4	2.9
	10	*Alare L*	2.5	3.0	**2.5**	**2.9**	**2.5**	**3.0**	2.4	2.9
	11	*Alare R*	2.3	3.0	**2.3**	**2.9**	**2.3**	**2.7**	2.3	2.8
	12	*Alar curvature point L*	2.7	3.8	**2.7**	**3.7**	**2.7**	**3.6**	2.7	3.9
	13	*Alar curvature point R*	2.5	3.1	**2.5**	**3.1**	**2.4**	**3.0**	2.4	2.9
	14	*Mid-nostril L*	2.5	3.0	**2.5**	**3.1**	**2.4**	**2.9**	2.4	2.9
	15	*Mid-nostril R*	2.5	3.0	**2.5**	**3.0**	**2.4**	**3.0**	2.4	2.9
	16	*Mid-columella L*	2.6	3.1	**2.6**	**3.0**	**2.6**	**3.1**	2.5	3.0
	17	*Mid-columella R*	2.4	3.4	**2.4**	**3.3**	**2.3**	**3.2**	2.3	3.3
	18	*Nasal depth L*	2.4	3.4	**2.3**	**3.4**	**2.3**	**3.2**	2.3	3.4
	19	*Nasal depth R*	2.5	3.0	**2.5**	**3.0**	**2.4**	**2.9**	2.4	2.9
		RMSEP	2.5	3.3	**2.5**	**3.2**	**2.5**	**3.1**	2.5	3.2

PE: Prediction errors on training data; PE_cv: prediction errors on non-trained data. Better predictions are indicated in bold.

Table 14
Prediction errors (in mm) of the predicted capulometric landmarks of the **nose** in the French sample, calculated on 108 individuals, based on training and on non-trained data.

French			Plain		Sex		Age		Sex*Age	
Predicted capulometric landmarks			PE	**PE**_cv	PE	**PE**_cv	PE	**PE**_cv	PE	**PE**_cv
Nose	**1**	*Pronasale*	3.0	3.5	**3.0**	**3.5**	**3.0**	**3.5**	2.9	3.4
	2	*Nasale inferius*	2.6	3.7	**2.6**	**3.7**	**2.6**	**3.5**	2.6	3.7
	3	*Columella*	2.9	3.5	**2.9**	**3.5**	**2.7**	**3.3**	2.7	3.3
	4	*Subnasale*	2.6	3.2	**2.6**	**3.1**	**2.5**	**3.2**	2.6	3.1
	5	*Sellion*	2.7	3.8	**2.7**	**3.9**	**2.7**	**3.7**	2.7	3.9
	6	*External alar curvature L*	2.9	3.6	**2.9**	**3.5**	**2.7**	**3.3**	2.7	3.3
	7	*External alar curvature R*	2.5	3.1	**2.5**	**3.1**	**2.5**	**3.1**	2.5	3.0
	8	*Superior alar curvature L*	2.8	3.9	**2.8**	**3.9**	**2.8**	**3.8**	2.8	4.0
	9	*Superior alar curvature R*	2.6	3.2	**2.6**	**3.2**	**2.5**	**3.0**	2.5	3.0
	10	*Alare L*	2.6	3.1	**2.6**	**3.0**	**2.6**	**3.1**	2.6	3.0
	11	*Alare R*	2.4	3.1	**2.4**	**3.0**	**2.4**	**2.8**	2.4	2.9
	12	*Alar curvature point L*	2.8	3.9	**2.8**	**3.8**	**2.8**	**3.7**	2.8	4.0
	13	*Alar curvature point R*	2.6	3.2	**2.6**	**3.6**	**2.5**	**3.1**	2.5	3.0
	14	*Mid-nostril L*	2.6	3.1	**2.6**	**3.2**	**2.5**	**3.0**	2.5	3.0
	15	*Mid-nostril R*	2.6	3.1	**2.6**	**3.1**	**2.5**	**3.1**	2.5	3.0
	16	*Mid-columella L*	2.7	3.2	**2.7**	**3.2**	**2.7**	**3.2**	2.6	3.1
	17	*Mid-columella R*	2.5	3.5	**2.5**	**3.4**	**2.4**	**3.3**	2.4	3.4
	18	*Nasal depth L*	2.5	3.5	**2.5**	**3.5**	**2.4**	**3.3**	2.4	3.5
	19	*Nasal depth R*	2.6	3.1	**2.6**	**3.1**	**2.5**	**3.0**	2.5	3.0
		RMSEP	2.6	3.4	**2.6**	**3.4**	**2.6**	**3.3**	2.6	3.3

PE: Prediction errors on training data; PE_cv: prediction errors on non-trained data. Better predictions are indicated in bold.

guidelines, tailored facial approximations that reflect regional variations in facial features improve identification outcomes. Our findings also advance forensic anthropology research by providing insights into the relationship between hard and soft tissue in facial morphology. Integrating these models into training programs may enhance proficiency in facial approximation techniques and victim identification,

Table 15
Prediction errors (in mm) of the predicted capulometric landmarks of the **mouth** in the white South African sample, calculated on 76 individuals, based on training and on non-trained data.

White South African			Plain		Sex		Age		Sex*Age	
Predicted capulometric landmarks			PE	**PE**_cv	PE	**PE**_cv	PE	**PE**_cv	PE	**PE**_cv
Mouth	**1**	*Chelion L*	3.6	3.5	3.0	3.5	**3.0**	**3.5**	2.9	3.4
	2	*Chelion R*	3.6	4.0	2.9	4.0	**2.9**	**3.8**	2.9	4.0
	3	*Labiale superius*	3.6	3.8	3.2	3.8	**3.0**	**3.6**	3.0	3.6
	4	*Labiale inferius*	3.6	3.5	2.9	3.4	**2.8**	**3.5**	2.9	3.4
	5	*Vermillion superius L*	3.6	4.1	3.0	4.2	**3.0**	**4.0**	3.0	4.2
	6	*Vermillion superius R*	3.6	3.9	3.2	3.8	**3.0**	**3.6**	3.0	3.6
	7	*Vermillion inferius L*	3.6	3.4	2.8	3.4	**2.8**	**3.4**	2.8	3.3
	8	*Vermillion inferius R*	3.6	4.2	3.1	4.2	**3.1**	**4.1**	3.1	4.3
		RMSEP	3.6	3.8	3.0	3.8	**3.0**	**3.7**	3.0	3.7

PE: Prediction errors on training data; PE_cv: prediction errors on non-trained data. Better predictions are indicated in bold.

Table 16
Prediction errors (in mm) of the predicted capulometric landmarks of the **mouth** in the French sample, calculated on 108 individuals, based on training and on non-trained data.

French			Plain		Sex		Age		Sex*Age	
Predicted capulometric landmarks			PE	**PE**_cv	PE	**PE**_cv	PE	**PE**_cv	PE	**PE**_cv
Mouth	**1**	*Chelion L*	3.6	3.1	2.7	3.1	**2.7**	**3.1**	2.6	3.0
	2	*Chelion R*	3.6	4.2	3.1	4.1	**3.1**	**4.0**	3.1	4.3
	3	*Labiale superius*	3.6	3.5	2.9	3.5	**2.8**	**3.4**	2.8	3.3
	4	*Labiale inferius*	3.6	3.4	2.9	3.5	**2.8**	**3.3**	2.8	3.3
	5	*Vermillion superius L*	3.6	3.4	2.9	3.4	**2.8**	**3.4**	2.8	3.3
	6	*Vermillion superius R*	3.6	3.5	3.0	3.5	**3.0**	**3.5**	2.9	3.4
	7	*Vermillion inferius L*	3.6	3.8	2.8	3.7	**2.7**	**3.6**	2.7	3.7
	8	*Vermillion inferius R*	3.6	3.8	2.8	3.8	**2.7**	**3.6**	2.7	3.8
		RMSEP	3.6	3.6	2.9	3.6	**2.8**	**3.5**	2.8	3.5

PE: Prediction errors on training data; PE_cv: prediction errors on non-trained data. Better predictions are indicated in bold.

Table 17
Population dependent quality of prediction (mm) of the predicted capulometric landmarks, calculated on 184 individuals, on the training and on non-trained data.

Population dependent quality of prediction	French predictions based on White SA sample data		White SA predictions based on French sample data	
	PE	**PE**_cv	PE	**PE**_cv
RMSEP	5.3	12.2	4.8	10.5

PE: Prediction errors on training data; PE_cv: prediction errors on non-trained data.

improving forensic investigation quality. Understanding the impact of population affinity on facial morphology underscores the need for tailored assessment guidelines, reducing prediction errors across diverse demographic groups. Moreover, integrating sex-specific and age-related predictors into biometric technology enhances accuracy and reliability across different demographics. In summary, these predictive models drive advancements in facial approximation and forensic anthropology, improving the accuracy of soft-tissue facial estimations and deepening our understanding of demographic influences on facial morphology for enhanced forensic outcomes.

Funding

This study was funded by the University of Pretoria in South Africa through the UP Postgraduate Masters Research Bursary.

CRediT authorship contribution statement

Alison Ridel: Writing – review & editing, Writing – original draft, Visualization, Validation, Software, Methodology, Investigation, Formal analysis, Data curation, Conceptualization. **Ericka L'Abbé:** Writing – review & editing, Writing – original draft, Visualization, Formal analysis, Data curation, Conceptualization. **Thandolwethu Mbali Mbonani:** Writing – review & editing, Writing – original draft, Visualization, Validation, Methodology, Investigation, Funding acquisition, Formal analysis, Data curation, Conceptualization.

Declaration of Competing Interest

none

Acknowledgements

We express our profound gratitude to Prof. Uys and Dr. Botha of the Oral and Dental Hospital and Groenkloof Hospital at the University of Pretoria, South Africa, for graciously providing access to their CBCT datasets. Additionally, we extend our appreciation to Dr. Heuze from the Pellegrin Hospital Group, Bordeaux, France for the invaluable contribution of French CBCT data, integral to the Bakeng se Afrika initiative. Special recognition is also extended to Meg-Kyla Erasmus for authorizing the utilization of shape data derived from a prior study conducted at the University of Pretoria.

References

[1] Mashigo L. There are an estimated 7 000 unidentified bodies in South Africa's medico-legal laboratories. Independent Online. Available from: ⟨https://www.iol.co.za/the-star/news/there-are-are-an-estimated-7-000-unidentified-bodies-in-south-africas-medico-legal-laboratories-7f419c2c-69e8-4fe5-863e-bc855f9cc008⟩; 2023.
[2] S.V. Tedeschi-Oliveira, R.F.H. Melani, N.H. De Almeida, L.A.S. De Paiva, Facial soft tissue thickness of Brazilian adults, 127.e1-127.e7, Forensic Sci. Int 193 (2009), https://doi.org/10.1016/j.forsciint.2009.09.002.
[3] Gerasimov M.M. Vosstanovlieniia Litsa po Cherapu; Gos Izd-vo Sovetskaia [The reconstruction of the face on the skull]. Unpublished translation. 1975 by Tshernezky;1955.

[4] Prag J., Neave R. Making faces: using forensic and archaeological evidence. 1. Publ. London: British Museum Press; 1997.
[5] Wilkinson C. Forensic facial reconstruction. Cambridge, UK, New York: Cambridge University Press; 2004.
[6] J.G. Clement, M.K. Marks, Computer graphic facial reconstruction, Elsevier, London, 2006.
[7] V. Bruce, G.W. Humphreys, Recognizing objects and faces, Vis. Cogn. 1 (1994) 141–180, https://doi.org/10.1080/13506289408402299.
[8] W. Zhao, R. Chellappa, P.J. Phillips, A. Rosenfeld, Face recognition: A literature survey, ACM Comput. Surv. 35 (2003) 399–458, https://doi.org/10.1145/954339.954342.
[9] H.F. Dorfling, Z. Lockhat, S. Pretorius, M. Steyn, A.C. Oettlé, Facial approximations: Characteristics of the eye in a South African sample, Forensic Sci. Int 286 (2018) 46–53, https://doi.org/10.1016/j.forsciint.2018.02.029.
[10] C.N. Stephan, P.L. Davidson, The placement of the human eyeball and canthi in craniofacial identification, J. Forensic Sci. 53 (2008) 612–619, https://doi.org/10.1111/j.1556-4029.2008.00718.x.
[11] N.D. Haig, The effect of feature displacement on face recognition, Perception 42 (2013) 1158–1165, https://doi.org/10.1068/p130505n.
[12] P. Guyomarc'h, B. Dutailly, C. Couture, H. Coqueugniot, Anatomical placement of the human eyeball in the orbit—validation using CT scans of living adults and prediction for facial approximation, J. Forensic Sci. (5) (2012) 1271–1275, https://doi.org/10.1111/j.1556-4029.2012.02075.x.
[13] S.-R. Kim, K.-M. Lee, J.-H. Cho, H.-S. Hwang, Three-dimensional prediction of the human eyeball and canthi for craniofacial reconstruction using cone-beam computed tomography, Forensic Sci. Int 261 (2016) 164.e1–164.e8, https://doi.org/10.1016/j.forsciint.2016.01.031.
[14] K. Krishan, T. Kanchan, S. Thakur, A study of morphological variations of the human ear for its applications in personal identification, Egypt. J. Forensic Sci. 9 (2019) 6, https://doi.org/10.1186/s41935-019-0111-0.
[15] O. Rubio, V. Galera, M.C. Alonso, Morphological variability of the earlobe in a Spanish population sample, Homo 68 (2017) 222–235, https://doi.org/10.1016/j.jchb.2017.03.007.
[16] R. Purkait, External ear: An analysis of its uniqueness, Egypt J. Forensic Sci. 6 (2016) 99–107, https://doi.org/10.1016/j.ejfs.2016.0.
[17] C. Sforza, G. Grandi, M. Binelli, D.G. Tommasi, R. Rosati, V.F. Ferrario, Age- and sex-related changes in the normal human ear, Forensic Sci. Int. 187 (2009) 110.e1–110.e7, https://doi.org/10.1016/j.forsciint.2009.02.019.
[18] R. Purkait, P. Singh, A test of individuality of human external ear pattern: Its application in the field of personal identification, Forensic Sci. Int. 178 (2008) 112–118, https://doi.org/10.1016/j.forsciint.2008.02.009.
[19] P. Guyomarc'h, C.N. Stephan, The Validity of Ear Prediction Guidelines Used in Facial Approximation, J. Forensic Sci. 57 (2012) 1427–1441, https://doi.org/10.1111/j.1556-4029.2012.02181.x.
[20] B. Swift, G.N. Rutty, The human ear: its role in forensic practice, J. Forensic Sci. 48 (2003) 2002251, https://doi.org/10.1520/JFS2002251.
[21] L.A. Thompson, J. Malmberg, N.K. Goodell, R.L. Boring, The distribution of attention across a Talker's face, Discourse Process. 38 (2004) 145–168, https://doi.org/10.1207/s15326950dp3801_6.
[22] C.M. Wilkinson, M. Motwani, E. Chiang, The relationship between the soft tissues and the skeletal detail of the mouth, J. Forensic Sci. 48 (2003) 728–732.
[23] C.N. Stephan, M. Henneberg, Predicting mouth width from inter-canine width–a 75% rule. J. Forensic Sci. 48 (2003) 725–727.
[24] C. Wilkinson, Facial reconstruction – anatomical art or artistic anatomy? J. Anat. 216 (2) (2010) 235–250, https://doi.org/10.1111/j.1469-7580.2009.01182.x.
[25] A.F. Ridel, F. Demeter, E.N. L'abbé, D. Vandermeulen, A.C. Oettlé, Nose approximation among South African groups from cone-beam computed tomography (CBCT) using a new computer-assisted method based on automatic landmarking, Forensic Sci. Int. 313 (2020) 110357, https://doi.org/10.1016/j.forsciint.2020.110357.
[26] O. Bulut, C.-Y.J. Liu, S. Gurcan, B. Hekimoglu, Prediction of nasal morphology in facial reconstruction: Validation and recalibration of the Rynn method, Leg. Med. 40 (2019) 26–31, https://doi.org/10.1016/j.legalmed.2019.07.002.
[27] S.L. Davy-Jow, S.J. Decker, J.M. Ford, A simple method of nose tip shape validation for facial approximation, Forensic Sci. Int. 214 (2012) 208.e1–208.e3, https://doi.org/10.1016/j.forsciint.2011.07.039.
[28] K.-M. Lee, W.-J. Lee, J.-H. Cho, H.-S. Hwang, Three-dimensional prediction of the nose for facial reconstruction using cone-beam computed tomography, Forensic Sci. Int. 236 (2014) 194.e1–194.e5, https://doi.org/10.1016/j.forsciint.2013.12.035.
[29] C.N. Stephan, M. Henneberg, W. Sampson, Predicting nose projection and pronasale position in facial approximation: A test of published methods and proposal of new guidelines, Am. J. Phys. Anthr. 122 (3) (2003) 240–250, https://doi.org/10.1002/ajpa.10300.
[30] S. Damas, O. Cordón, O. Ibáñez, Handbook on Craniofacial Superimposition: The MEPROCS Project, Springer International Publishing, Cham, 2020, https://doi.org/10.1007/978-3-319-11137-7.
[31] T. Balueva, E. Veselovskaya, L. Valencia-Caballero, et al., Nuevos estudios en el area de reconstruccion facial a partir de datos craneologicos, Rev. Esp. De. Antropol. Fis. 11 (2009) 22.
[32] L. Verzé, History of facial reconstruction, Acta Biomed. 80 (2009) 5–12.
[33] S.E. Whitnall, Henry Frowde. The Anatomy of the Human Orbit and Accessory Organs of Vision, Oxford Medical Publications, London, 1921.
[34] R.M. George, Anatomical and artistic guidelines for forensic facial reconstruction, in: M.Y. Iscan, R.P. Helmer (Eds.), In Forensic Analysis of the Skull, Wiley Liss Inc, New York, 1993, pp. 215–227.
[35] D.A. Rudee, Proportional profile changes concurrent with orthodontic therapy, Am. J. Orthod. 50 (1964) 421–434, https://doi.org/10.1016/0002-9416(64)90205-2.
[36] M. Faysal Talass, L. Tollaae, R.C. Baker, Soft-tissue profile changes resulting from retraction of maxillary incisors, Am. J. Orthod. Dentofac. Orthop. 91 (1987) 385–394, https://doi.org/10.1016/0889-5406(87)90391-X.
[37] N. Renwick, Ear lobe morphology and its relationship to the mastoid process. Centre for Anatomy and Human Identification, University of Dundee, Dundee, The Online Journal of CAHId, AXIS, 2012.
[38] D.E. Lieberman, B.M. McBratney, G. Krovitz, The evolution and development of cranial form in Homo sapiens, Proc. Natl. Acad. Sci. USA 99 (3) (2002) 1134–1139, https://doi.org/10.1073/pnas.022440799.
[39] Y. Tomoyasu, T. Yamaguchi, A. Tajima, T. Nakajima, I. Inoue, K. Maki, Further evidence for an association between mandibular height and the growth hormone receptor gene in a Japanese population, Am. J. Orthod. Dentofac. Orthop. 136 (4) (2009) 536–541, https://doi.org/10.1016/j.ajodo.2007.10.054.
[40] F. Gröning, M. Fagan, P. O'higgins, Comparing the Distribution of Strains with the Distribution of Bone Tissue in a Human mandible: A Finite Element Study, Anat. Rec. (Hoboken) 296 (1) (2013) 9–18, https://doi.org/10.1002/ar.22597.
[41] P. Guyomarc'h, B. Dutailly, J. Charton, F. Santos, P. Desbarats, H. Coqueugniot, Anthropological facial approximation in three dimensions (AFA3D): computer-assisted estimation of the facial morphology using geometric morphometrics, J. Forensic Sci. 59 (6) (2014) 1502–1516, https://doi.org/10.1111/1556-4029.12547.
[42] M. Evison, I. Dryden, N. Fieller, X. Mallett, L. Morecroft, D. Schofield, et al., Key Parameters of Face Shape Variation in 3D in a Large Sample, J. Forensic Sci. 55 (2010) 159–162, https://doi.org/10.1111/j.1556-4029.2009.01213.x.
[43] N. Curtis, Craniofacial biomechanics: an overview of recent multibody modelling studies: Craniofacial biomechanics, J. Anat. 218 (2011) 16–25, https://doi.org/10.1111/j.1469-7580.2010.01317.x.
[44] S. Ousley, R. Jantz, D. Freid, Understanding race and human variation: Why forensic anthropologists are good at identifying race, Am. J. Phys. Anthr. 139 (2009) 68–76, https://doi.org/10.1002/ajpa.21006.
[45] A.D. Weinberger, Interracial Marrage—Its Statutory Prohibition, Genetic Import, and Incidence, J. Sex. Res. 2 (1966) 157–168, https://doi.org/10.1080/00224499.1966.10749561.
[46] M. Steyn, E.N. L'Abbé, J. Myburgh, Forensic Anthropology as Practiced in South Africa. Handbook of Forensic Anthropology and Archaeology., Routledge, London, 2016.
[47] J.T. Hefner, Cranial nonmetric variation and estimating ancestry, J. Forensic Sci. 54 (5) (2009) 985–995, https://doi.org/10.1111/j.1556-4029.2009.01118.x.
[48] M.K. Spradley, Metric Methods for the Biological Profile in Forensic Anthropology: Sex, Ancestry, and Stature, Acad. Forensic Pathol. 6 (2016) 391–399, https://doi.org/10.23907/2016.040.
[49] P. Mitteroecker, S. Windhager, G.B. Müller, K. Schaefer, The Morphometrics of "Masculinity" in Human Faces, PLoS ONE 10 (2015) e0118374, https://doi.org/10.1371/journal.pone.0118374.
[50] R.J. Hennessy, S. McLearie, A. Kinsella, J.L. Waddington, Facial surface analysis by 3D laser scanning and geometric morphometrics in relation to sexual dimorphism in cerebral–craniofacial morphogenesis and cognitive function, J. Anat. 207 (2005) 283–295, https://doi.org/10.1111/j.1469-7580.2005.00444.x.
[51] O. Agbolade, A. Nazri, R. Yaakob, A.A. Ghani, Y.K. Cheah, Morphometric approach to 3D soft-tissue craniofacial analysis and classification of ethnicity, sex, and age, PLoS ONE 15 (2020) e0228402, https://doi.org/10.1371/journal.pone.0228402.
[52] G.C. Krüger, E.N. L'Abbé, K.E. Stull, M.W. Kenyhercz, Sexual dimorphism in cranial morphology among modern South Africans, Int J. Leg. Med 129 (2015) 869–875, https://doi.org/10.1007/s00414-014-1111-0.
[53] E.N. L'Abbé, M. Kenyhercz, K.E. Stull, N. Keough, S. Nawrocki, Application of Fordisc 3.0 to Explore Differences Among Crania of North American and South African Blacks and Whites, J. Forensic Sci. 58 (2013) 1579–1583, https://doi.org/10.1111/1556-4029.12198.
[54] D.H. Enlow, M.G. Hans, Essentials of facial growth, Saunders, Philadelphia, 1996.
[55] M.A. McCollum, Nasomaxillary remodeling and facial form in robust Australopithecus: a reassessment, J. Hum. Evol. 54 (2008) 2–14, https://doi.org/10.1016/j.jhevol.2007.05.013.
[56] M. Bastir, A. Rosas, Hierarchical nature of morphological integration and modularity in the human posterior face, Am. J. Phys. Anthr. 128 (2005) 26–34, https://doi.org/10.1002/ajpa.20191.
[57] A.M. Albert, K. Ricanek, E. Patterson, A review of the literature on the aging adult skull and face: Implications for forensic science research and applications, Forensic Sci. Int 172 (2007) 1–9, https://doi.org/10.1016/j.forsciint.2007.03.015.
[58] Neave RAH, Age changes in the face in adulthood, in: J.G. Clement, D.L. Ranson (Eds.), Craniofacial Identification in Forensic Medicine, Arnold Publications, Sydney, 1998, pp. 215–231.
[59] C.F. Spoor, F.W. Zonneveld, G.A. Macho, Linear measurements of cortical bone and dental enamel by computed tomography: Applications and problems, Am. J. Phys. Anthr. 91 (1993) 469–484, https://doi.org/10.1002/ajpa.1330910405.
[60] P.J. Schneider, D. Eberly, Geometric tools for computer graphics, Elsevier Science Inc, New York, USA, 2002.
[61] P. Mitteroecker, P. Gunz, Advances in geometric morphometrics, Evol. Biol. 36 (2) (2009) 235–247, https://doi.org/10.1007/s11692-009-9055-x.
[62] G. Ocakoğlu, S. Turan Özdemİr, İ. Ercan, A. Etöz, The shape of the external human ear: A geometric morphometric study, Turk. Klin. J. Med Sci. 33 (1) (2013) 184–190, https://doi.org/10.5336/medsci.2012-30150.
[63] Schlager S. Soft-tissue reconstruction of the human nose: population differences and sexual dimorphism = Weichteilrekonstruktion der menschlichen Nase:

Populationsunterschiede und Sexualdimorphismus. PhD. Universität Freiburg; 2013.
[64] J. Caple, C.N. Stephan, A standardized nomenclature for craniofacial and facial anthropometry, Int J. Leg. Med 130 (3) (2016) 863–879, https://doi.org/10.1007/s00414-015-1292-1.
[65] White T.D., Folkens P.A. The human bone manual. Amsterdam, Boston: Elsevier Academic; 2005.
[66] V.F. Ferrario, C. Sforza, A. Anderbegani, C.E. Poggio, L.L. Dalloca, Relative position of porion and tragus in orthodontic patients, Clin. Anat. 8 (5) (1995) 352–358, https://doi.org/10.1002/ca.980080508.
[67] F. Lundström, A. Lundström, Natural head position as a basis for cephalometric analysis, Am. J. Orthod. Dentofac. Orthop. 101 (3) (1992) 244–247, https://doi.org/10.1016/0889-5406(92)70093P.
[68] A.F. Ridel, F. Demeter, M. Galland, E.N. L'abbé, D. Vandermeulen, A.C. Oettlé, Automatic landmarking as a convenient prerequisite for geometric morphometrics. Validation on cone beam computed tomography (CBCT)- based shape analysis of the nasal complex, Forensic Sci. Int 306 (2020) 110095, https://doi.org/10.1016/j.forsciint.2019.110095.
[69] M.-K. Erasmus, E.N. L'Abbé, A.F. Ridel, A geometric morphometric assessment of the hard tissue external auditory meatus and soft tissue ear of South Africans, Forensic Sci. Int Rep. 8 (2023) 100331, https://doi.org/10.1016/j.fsir.2023.100331.
[70] T. Mbonani, A. Hagg, E. L'Abbé, A. Oettlé, A. Ridel, Validation of the utilisation of automatic placement of anatomical and sliding landmarks on three-dimensional models for shape analysis of human pelves, Forensic Imaging 33 (2023) 200542, https://doi.org/10.1016/j.fri.2023.200542.
[71] P. Claes, D. Vandermeulen, S. De Greef, G. Willems, J.G. Clement, P. Suetens, Computerized craniofacial reconstruction: conceptual framework and review, Forensic Sci. Int 201 (1-3) (2010) 138–145, https://doi.org/10.1016/j.forsciint.2010.03.008.
[72] D.G. Kendall, Shape manifolds, procrustean metrics, and complex projective spaces, Bull. Lond. Math. Soc. 16 (2) (1984) 81–121, https://doi.org/10.1112/blms/16.2.81.
[73] D.E. Slice, Geometric morphometrics, Annu Rev. Anthr. 36 (1) (2007) 261–281, https://doi.org/10.1146/annurev.anthro.34.081804.120613.
[74] Dryden I.L., Mardia K.V. Statistical shape analysis with applications in R. 2nd ed. Chichester, UK; Hoboken. NJ: John Wiley & Sons; 2016.
[75] J.C. Gower, Generalized Procrustes analysis, Psychometrika 40 (1) (1975) 33–51, https://doi.org/10.1007/BF02291478.
[76] F.J. Rohlf, D. Slice, Extensions of the Procrustes method for the optimal superimposition of landmarks, Syst. Zool. 39 (1) (1990) 40, https://doi.org/10.2307/2992207.
[77] P. Mitteroecker, P. Gunz, S. Windhager, K. Schaefer, A brief review of shape, form, and allometry in geometric morphometrics, with applications to human facial morphology, Hystrix Ital. J. Mammal. 24 (2013), https://doi.org/10.4404/hystrix-24.1-6369.
[78] Martens H., Naes T. Multivariate calibration [reprint]. Chichester: Wiley; 2002.
[79] S. Wold, M. Sjöström, L. Eriksson, PLS-regression: a basic tool of chemometrics, Chemom. Intell. Lab Syst. 58 (2) (2001) 109–130, https://doi.org/10.1016/S0169-7439(01)00155-1.
[80] H. Abdi, Partial least squares regression and projection on latent structure regression (PLS Regression), WIREs Comp. Stat. 2 (1) (2010) 97–106, https://doi.org/10.1002/wics.51.
[81] B.-H. Mevik, H.R. Cederkvist, Mean squared error of prediction (MSEP) estimates for principal component regression (PCR) and partial least squares regression (PLSR), J. Chemom. 18 (9) (2004) 422–429, https://doi.org/10.1002/cem.887.
[82] J. Djordjevic, A.I. Zhurov, S. Richmond, Visigen Consortium, Genetic and environmental contributions to facial morphological variation: A 3D population-based twin study, PLOS ONE 11 (9) (2016) e0162250, https://doi.org/10.1371/journal.pone.0162250.
[83] A.C. Oettlé, F.P. Demeter, E.N. L'abbé, Ancestral variations in the shape and size of the zygoma, Anat. Rec. (Hoboken) 300 (1) (2017) 196–208, https://doi.org/10.1002/ar.23469.
[84] Paschetta, C. De Azevedo, S. Castillo, L. Martínez-Abadías, N. Hernández, M. Lieberman DE, et al., The influence of masticatory loading on craniofacial morphology: A test case across technological transitions in the Ohio valley, Am. J. Phys. Anthr. 141 (2) (2010) 297–314, https://doi.org/10.1002/ajpa.21151.
[85] E. Cunha, D.H. Ubelaker, Evaluation of ancestry from human skeletal remains: a concise review, Forensic Sci. Res 5 (2) (2020) 89–97, https://doi.org/10.1080/20961790.2019.1697060.
[86] E.N. L'Abbé, C. Van Rooyen, S.P. Nawrocki, P.J. Becker, An evaluation of non-metric, cranial traits used to estimate ancestry in a South African sample., 195.e1-7, Forensic Sci. Int 209 (1-3) (2011), https://doi.org/10.1016/j.forsciint.2011.04.002.
[87] K. Imaizumi, K. Taniguchi, Y. Ogawa, K. Matsuzaki, H. Maekawa, T. Nagata, et al., Three-dimensional shape variation and sexual dimorphism of the face, nose, and mouth of Japanese individuals, Forensic Sci. Int 302 (2019) 109878, https://doi.org/10.1016/j.forsciint.2019.109878.
[88] P. Claes, M. Walters, D. Gillett, D. Vandermeulen, J.G. Clement, P. Suetens, The normal-equivalent: a patient-specific assessment of facial harmony, Int J. Oral. Maxillofac. Surg. 42 (9) (2013) 1150–1158, https://doi.org/10.1016/j.ijom.2013.03.011.
[89] Y. Takema, Y. Yorimoto, M. Kawai, et al., Age-related changes in the elastic properties and thickness of human facial skin, Br. J. Dermatol. 131 (1994) 641–648.
[90] F. Bodic, L. Hamel, E. Lerouxel, et al., Bone loss and teeth, Jt. Bone Spine 72 (2005) 215–221.
[91] F.M. Tilotta, J.A. Glaunès, F.J.P. Richard, Y. Rozenholc, A local technique based on vectorized surfaces for craniofacial reconstruction, Forensic Sci. Int 200 (2010) 50–59, https://doi.org/10.1016/j.forsciint.2010.03.029.
[92] D. Vandermeulen, P. Claes, D. Loeckx, S. De Greef, G. Willems, P. Suetens, Computerized craniofacial reconstruction using CT-derived implicit surface representations, Forensic Sci. Int 159 (Suppl 1) (2006) S164–S174, https://doi.org/10.1016/j.forsciint.2006.02.036.